Fast computation of radio wave propagation effects

Thomas Mejstrik*, Taulant Berisha†, Sebastian Woblistin‡

***Abstract*—UAV operations are quickly gaining ground due to rapid global market penetration. While on one hand, novel technologies that bridge communication networks to aviation industry are yet to be explored, on the other hand, their development requires highly scalable systems to enable BVLoS missions. This requirement imposes a big bottleneck in terms of computation complexity. This paper presents a method for fast computation of multiple diffraction of radio waves over knife-edge obstacles based on the Deygout technique and some offline computation steps, including a ground profile analysis. No rigorous results for such an analysis are known yet. We prove that this algorithm is equivalent to the original Deygout algorithm for all non-line-of-sight points, and show heuristics confirming that it is mostly applicable in the line-of-sight case. With small modifications our method is also applicable to the Epstein-Peterson technique and the Giovanelli technique.**

***Index Terms*—Estimation, Diffraction, Electromagnetic wave propagation, Algorithms, Mobile communication**

I. Introduction

Delivery of small packages, including medical supplies, fire fighting support and infrastructure inspection, represent great commercial potential for communication providers. Due to the growth in the unmanned aerial vehicle (UAV) market, cellular networks are playing a key role to facilitate and enable beyond visual line-of-sight (BVLoS) operations [1]. In this regard, safety authorities and air traffic regulators have identified the availability of a command & control (C2) link as a prerequisite for integration of UAVs into the airspace [2], [3]. C2 link owns exclusive responsibility to enable such operations and represents a critical chunk to perform reliable data delivery.

While on one hand, cellular operators want to keep full control of their network in 3D airspace – similarly as to terrestrial communications, on the other hand due to safety reasons, air traffic regulators must be aware of UAV's flight mission and telemetry data, as well as command-and-control data. Therefore, an interface enabling data exchange between the two parties is a required linkage. To enable BVLoS UAV operations, unmanned aircraft system traffic management (UTM) authority has defined several tasks among which software systems and data exchange protocols are key factors yet to be developed [4].

To our best of knowledge, the only solution in market that serves as a bridge connection between aviation industry and cellular operators is AirborneRF [5]. AirborneRF takes into account both national airspace control and the radio coverage delivered by the cellular network in real-time to control the UAV within a safe 3D corridor and reliably deliver C2 messages.

A. Computation complexity

An important aspect in cellular communication systems and development of novel technologies is computational complexity. Different to conventional systems, aviation management systems will require connectivity data nearly in real time. Development of efficient software functions and enabling reliable data exchange requires development of novel algorithms that run swiftly on the stack. Computation of radio wave propagation effects, such as small-scale fadings, diffraction, scattering, refraction, and reflections demand huge memory capacity, and thus, challenge parameter estimation for real-time applications. In particular, multiple diffraction of radio waves over several obstacles from a given ground profile requires development of fast computation techniques. Yet, no rigorous results are known in literature. To tackle this problem, we propose an offline computation step combined with a revised Deygout algorithm, both based on the Deygout technique.

B. Diffraction

Many classical approximations, like Bullington, Epstein-Peterson, Deygout, Giovanelli, for the computation of the diffraction loss of radio waves are built upon the so-called *single knife-edge case* [6]–[11].[1] A *knife-edge*, depicted in Figure 1, is an infinitely thin obstacle with infinite width; i.e. it extends infinitely into and out of the page. Consequently, the received energy decays due to lower number of rays being able to reach the receiver. Therefore, some of the rays radiated from the transmitter will not reach the receiver. However, according to the Huygens–Fresnel principle, each point at the wave-front can be considered as a secondary source of wavelets [15], which combine to form waves propagating toward the receiver to the right of the screen, even if there is non-line-of-sight (*NLoS*) between the transmitter and the receiver.

C. Organization

In *Section II* we present the formulas for the single knife-edge diffraction case and derive some useful properties. In *Section II-A* we prove the main Lemma II.6 of the paper

*Dimetor GmbH, Wiedner Hauptstraße 24/15, 1040 Vienna, Austria; Faculty of mathematics, University of Vienna, Universitätsring 1, 1010 Vienna, Austria; email: tommsch@gmx.at

†Dimetor GmbH, Wiedner Hauptstraße 24/15, 1040 Vienna, Austria; email: taulant.berisha@dimetor.com

‡Dimetor GmbH, Wiedner Hauptstraße 24/15, 1040 Vienna, Austria; email: sebastian.woblistin@dimetor.com

[1]Note though, in recent years new fast methods to compute the diffraction loss arose due to the advent of GPGPUs, making use of ray tracing and machine learning techniques, see e.g. [12]–[14].

giving rise to useful Corollaries, presented in Section II-A and II-B, which we base our revised Deygout algorithm on. In *Section III* we present the Deygout algorithm and the main statements for our revised algorithm in Theorems III.4 and III.5, Remark III.7 and Algorithm III.9. At the end we close the paper in Section IV.

II. Single knife-edge diffraction

The attenuation caused by a knife-edge shaped obstacle can be computed by [16, Chapter 4.2]

$$J(\tilde{\nu}) = -20\log_{10} F(\tilde{\nu}) \text{ [dB]}, \tag{1}$$

where the *Fresnel-Kirchhoff parameter* $\tilde{\nu}$, depending on the wavelength λ and the geometric parameters $\tilde{a}_O$, $\tilde{d}_R$, $\tilde{d}_O$, defined in Figure 1, is essentially the square-root of a first-order approximation of the difference between the lengths of the path $(T)-(O)-(R)$ going over the tip of the obstacle and the LoS path $(T)-(R)$, see Figure 1. It is given by

$$\tilde{\nu} = \tilde{a}_O \sqrt{\frac{2\tilde{d}_R}{\lambda \tilde{d}_O(\tilde{d}_R - \tilde{d}_O)}}, \tag{2}$$

and F is a *Fresnel integral* given by

$$F(\nu) = \frac{1+i}{2}\left(\int_\nu^\infty \cos\frac{r^2\pi}{2}\,dr - i\int_\nu^\infty \sin\frac{r^2\pi}{2}\,dr\right). \tag{3}$$

To derive the ν-parameter for the case when the altitude of the receiver a_R is non-zero, and under the assumptions

$$a_O \ll d_O, \quad a_R \ll d_R, \tag{4}$$

defined in Figure 1, we substitute in Equation (2), $\dfrac{y}{d_O} = \dfrac{a_R}{d_R}$, $\tilde{a}_O = a_O - y$, $\tilde{d}_O = d_O$, which gives rise to Definition II.1.

Definition II.1. Given an obstacle $O = (d_O, a_O)$ and a receiver $R = (d_R, a_R)$, $0 < d_O < d_R$, we define the *ν-parameter* by

$$\nu(O,R) = \nu(d_O, a_O, d_R, a_R) = \frac{a_O d_R - d_O a_R}{\sqrt{d_R d_O (d_R - d_O)}}, \tag{5}$$

where we dropped the constant factor $\sqrt{2/\lambda}$ silently to make the problem frequency independent.

Furthermore, if not stated otherwise, we assume the transmitter to be located at the origin, i.e. $T = (0,0)$.

Definition II.2. For $\nu > -0.78$ the function J_{ITU} is an approximation of $J = -20\log_{10} F$ defined by [17, Equation (31)]

$$J_{ITU}(\nu) = 6.9 + 20\log_{10}\Big(\sqrt{(\nu-0.1)^2+1} + \nu - 0.1\Big). \tag{6}$$

For $\nu \le -0.78$ we set $J_{ITU} \equiv 0$.

See Figure 2 for a plot of the functions J and J_{ITU}. Since J_{ITU} is monotone, it suffices to study the behaviour of the ν-parameter to make qualitative statements about the single knife-edge diffraction model and models derived from the single knife-edge diffraction model.

Lemma II.3. *The function J_{ITU} is strictly monotone increasing for $\nu > -0.78$.*

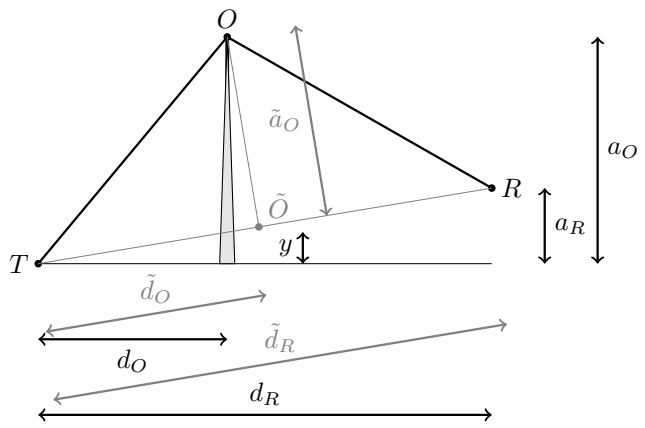

Fig. 1. T: Transmitter, R: Receiver, O: Obstacle of knife-edge type. Drawn in grey is the real setting, drawn in black the approximated one.

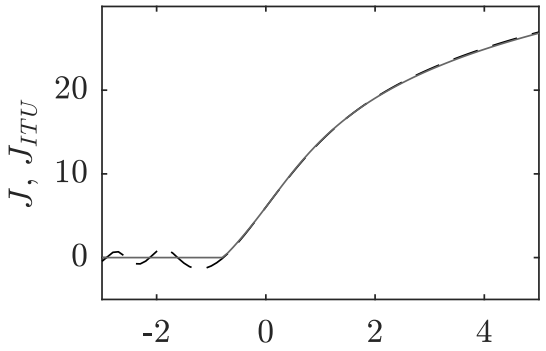

Fig. 2. The function J (dashed black line) and its approximation J_{ITU} (solid grey line) as defined by (1) and (6).

Proof.

$$\partial_\nu J_{ITU}|_\nu = \frac{200\log_{10} e}{\sqrt{100\nu^2 - 20\nu + 101}} > 0 \quad \text{for all } \nu \in \mathbb{R} \quad \square$$

A. Linearly moving receiver

In this chapter we lay the mathematical foundation to show that, in the generic case, the maximum attenuation caused by diffraction is attained on the boundary of a given region, in particular if the receiver is located on the ground.

Since the diffraction effects behave qualitatively different for line-of-sight (*LoS*) and non-line-of-sight points, we define the following vocabulary.

Definition II.4. We say a point is *LoS* if there is line-of-sight between the transmitter and the point. We say a point is *NLoS* if it is not LoS.

Using the ν-parameter one obtains a simple characterisation of LoS points.

Lemma II.5. *Given an obstacle $O = (d_O, a_O)$ and a point $R = (d_R, a_R)$. The point R is LoS if $\nu(O,R) < 0$. The point R is NLoS if $\nu(O,R) \ge 0$.*[2]

[2]The choice that a point R with $\nu(O,R) = 0$ is NLoS is high-handed but motivated by Lemma II.6.

Proof. Since the denominator of the ν parameter is always positive, its sign is defined by $a_O d_R - d_O a_R$, which proves the claim. □

We now prove a very useful lemma, which allows us to construct our *inverse Deygout algorithm* in Section III-A.

Lemma II.6. *The ν-parameter (corresponding to one fixed obstacle) has no local non-negative maxima on any straight line.*

Proof. Given an obstacle $O = (d_O, a_O)$, $d_O > 0$. We first consider the case when the line is vertical. For fixed d_R, $0 < d_O < d_R$, Equation (5) becomes

$$\nu(a_R) = \frac{a_O d_R}{\sqrt{d_R d_O (d_R - d_O)}} - \frac{d_O}{\sqrt{d_R d_O (d_R - d_O)}} a_R, \quad (7)$$

which is a linear function, and thus, proves the claim.

Now let $g(x) = g_0 + g_1 x$. We define

$$\nu_g(x) = \frac{a_O x - d_O g(x)}{\sqrt{x d_O (x - d_O)}} = \frac{a_O x - d_O (g_0 + g_1 x)}{\sqrt{x d_O (x - d_O)}}. \quad (8)$$

By Lemma II.5, a point $(x, g(x))$ is NLoS if and only if $\tilde{\nu}_g(x) \geq 0$. Let $B \geq 0$, any non-negative, NLoS, local maxima of $\tilde{\nu}_g$ satisfies

$$\begin{cases} \nu_g(x) \geq B & \text{(9a)} \\ \nu_g'(x) = 0 & \text{(9b)} \\ \nu_g''(x) \leq 0. & \text{(9c)} \end{cases}$$

This system simplifies under the assumption $0 < d_O < x$ to

$$\begin{cases} a_O x \geq B\sqrt{d_O x (x - d_O)} + d_O (g_0 + g_1 x) & \text{(10a)} \\ x(d_O g_1 + 2g_0 - a_O) = d_O g_0 & \text{(10b)} \\ (8g_0 + d_O g_1 - a_O) d_O x - 4(2g_0 + d_O g_1 - a_O) x^2 \leq 3 d_O^2 g_0 & \text{(10c)} \end{cases}$$

Equations (10c) and (10b) yield $d_O g_0 \geq 5 g_0 x$ which is only possible if $g_0 \leq 0$, since $0 < d_O < x$. Equations (10a) and (10b) yield $B \leq 2g_0\sqrt{\frac{x - d_O}{d_O x}}$, which is only possible if $B \leq 0$, since $0 < d_O < x$ and $g_0 \leq 0$. By assumption $B \geq 0$, and thus, $B = 0$.

Now, if $B = 0$, then $0 \leq g_0 \leq 0$, and thus, $a_0 \geq d_0 g_1$ which is exactly the case between NLoS and LoS which we defined to be NLoS. □

Example II.7. The NLoS condition, i.e. the non-negativity of the local extrema or the condition $B \geq 0$ in the proof of Theorem II.6, is a necessary condition as the following example shows. Indeed, for the obstacle $O = (1, -5/2)$ and the linear function $h(x) = -1 - x$ the function $\tilde{\nu}_h$ attains a local maxima $-\sqrt{2}$ at $x = 2$, and the corresponding point $(2, h(2))$ is LoS.

Lemma II.6 gives rise to some useful Corollaries.

Corollary II.8. *Given an obstacle $O = (d_O, a_O)$, $d_O > 0$, and a piece-wise linear function $r(x)$ defined on $x > d_O$. The function $\nu_r(x) = \nu(d_O, a_O, x, r(x))$ has non-negative local maxima only at the end points of the line segments of the function.*

Due to the symmetry of Equation (5) of the ν-parameter, a dual statement for linearly moving obstacles holds.

Corollary II.9. *Given a receiver $R = (d_R, a_R)$ and a piece-wise linear function $o(x)$ defined on $0 < x < d_R$. The function $\nu_o(x) = \nu(x, o(x), d_R, a_R)$ has non-negative local maxima only at the end points of the line segments of the function.*

Since we are not restricted to move on straight lines only, Corollary II.10 follows.

Corollary II.10. *Given an obstacle $O = (d_O, a_O)$, $d_O > 0$, a closed, non-empty domain $D \subseteq \mathbb{R}^2$, $d_x > d_O$ for all $d = (d_x, d_y) \in D$, such that there exists $\tilde{d} \in D$ with $\nu(\tilde{d}) > 0$. Then, the ν-parameter attains its maximum at ∂D.*

Proof. Assume there exists $d^\circ \in D^\circ$ such that $\nu(d^\circ) = \max_{d \in D} \nu(d)$. By assumption, $\nu(d^\circ) > 0$, i.e. d° is NLoS. Thus, there exists a straight line g through d° which is still contained in D°. Therefore, the function ν_g attains a local maximum which is a contradiction to Theorem II.6. □

B. Multiple obstacles

In the next few corollaries we are interested in the question, which of multiple obstacles yields the largest ν parameter, respectively diffraction loss.

Definition II.11. Given a set of obstacles $O_j = (d_{O_j}, a_{O_j})$, $j = 1, \ldots, J$ and a receiver $R = (d_R, a_R)$ with $d_{O_i} < d_{O_j} < d_R$ for all $i < j$. We say O_i is a main obstacle for R if $\nu(O_i, R) \geq \nu(O_j, R)$ for all $j = 1, \ldots, J$.

An obstacle shadowed by other obstacles cannot be a main obstacle if the receiver is NLoS.

Corollary II.12. (a) *There does not exist a configuration such that for three obstacles $O_1 = (d_{O_1}, a_{O_1})$, $O_2 = (d_{O_2}, a_{O_2})$, $O_3 = (d_{O_3}, a_{O_3})$, and a transmitter $R = (d_R, a_R)$, the following holds true:*

$$\begin{cases} 0 < d_{O_1} < d_{O_2} < d_{O_3} < d_R \\ a_{O_2} < \frac{a_{O_1}(d_{O_3} - d_{O_2}) + a_{O_3}(d_{O_2} - d_{O_1})}{d_{O_3} - d_{O_1}} \\ 0 < \nu(O_1, R) < \nu(O_2, R) \wedge 0 < \nu(O_3, R) < \nu(O_2, R) \end{cases}.$$

In other words, the main NLoS obstacle is always on the upper boundary of the convex hull of the points defined by the transmitter, obstacles and the receiver.

(b) *If the NLoS condition is dropped, then (a) is false.*

Proof. The second condition states that the height of the second obstacle is below the line defined by obstacles O_1 and O_2. Therefore, by Corollary II.9, $\nu(O_2, R) < \max\{\nu(O_1, R), \nu(O_2, R)\}$.

(b) Given $O_1 = (13, 1)$, $O_2 = (24, 10)$, $O_3 = (32, 20)$, $R = (33, 24)$. It follows that $\nu(O_1, R) \simeq -3.01$, $\nu(O_2, R) \simeq -2.91$ and $\nu(O_3, R) \simeq -3.32$, see Figure 3. □

Remark II.13. A similar statement to Corollary II.12 (a) also holds for LoS-points. Namely, given two obstacles $O_1 =$

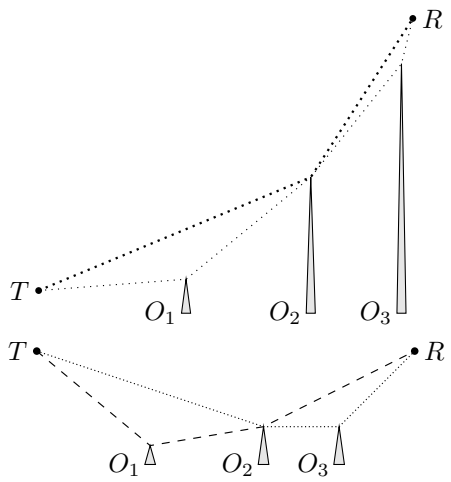

Fig. 3. (first) Illustration of counter example in Corollary II.12 (b). (second) Illustration of obstacles defined in Remark II.13.

(d_{O_1}, a_{O_1}), $O_2 = (d_{O_2}, a_{O_2})$, and a receiver $R = (d_R, a_R)$, there does not exists configuration such that

$$\begin{cases} 0 < d_{O_1} < d_{O_2} < d_R \\ \frac{a_R - a_{O_2}}{d_R - d_{O_2}} < \frac{a_{O_2} - a_{O_1}}{d_{O_2} - d_{O_1}} \\ 0 < \nu(O_2, R) < \nu(O_1, R) \end{cases}$$

or

$$\begin{cases} 0 < d_{O_1} < d_{O_2} < d_R \\ \frac{a_{O_2} - a_{O_1}}{d_{O_2} - d_{O_1}} < \frac{a_{O_1}}{d_{O_1}} \\ 0 < \nu(O_1, R) < \nu(O_2, R) \end{cases}.$$

Though, the use of such a theorem is limited, since the "LoS-hull" is not convex in general. E.g. given $O_1 = (1.5, -1.25)$, $O_2 = (3, -1)$, $O_3 = (4, -1)$, $R = (5, 0)$, the "LoS-hull" is the union of the two hulls $(T - O_1 - O_2 - R)$ and $(T - O_2 - O_3 - R)$, and thus, not convex anymore.

The main obstacle of a receiver right above of another receiver has either the same main obstacle or a main obstacle which lies left of the main obstacle of the lower receiver.

Corollary II.14. (a) *Given obstacles $O_j = (d_{O_j}, a_{O_j})$, $j = 1, \ldots, J$ and receivers $R_1 = (d_R, a_{R_1})$, $R_2 = (d_R, a_{R_2})$ such that $d_{O_i} < d_{O_j} < d_R$ for all $i < j$ and $a_{R_1} < a_{R_2}$. Then, the main obstacle of R_2 lies left of the main obstacle of R_1, or it is the same.*

(b) *A similar statement for horizontally moving receivers is wrong.*

Proof. (a) This follows directly from Corollary II.12 or from Corollary II.14.

(b) Let $O_1 = (2, 15)$, $O_2 = (3.2, 20.5)$ and we fix our receivers at height $a_R = 20.3$. It is not hard to see that $\lim_{d_R \to d_{O_2}} \nu(O_2, R) = \infty$, but, $\lim_{d_R \to d_{O_2}} \nu(O_1, R) < \infty$. Furthermore, $\lim_{d_R \to \infty} \nu(O_2, R) = \frac{a_{O_2}}{\sqrt{d_{O_2}}} \simeq 11.5$, but $\lim_{d_R \to \infty} \nu(O_1, R) = \frac{a_{O_1}}{\sqrt{d_{O_1}}} \simeq 10.6$.

Thus, for small enough and large enough d_R (i.e. $3.2 < d_R < 3.20908$ or $d_R > 3.48071$), the main obstacle for a receiver is O_2, and, for all receivers in between, e.g. $R_2 = (3.4, a_R)$, $\nu(O_1, R_2) \simeq 3.24 > 2.78 \simeq \nu(O_2, R_2)$ the first obstacle is the main obstacle. □

By Remark II.15, in the general case a configuration like the one in the proof of II.14 (b) will either not occur or the ν-parameter corresponding to the main obstacle is only slightly larger than the ν-parameters of other obstacles. Thus, for real world examples we may assume that II.14 (b) is true.

Remark II.15. By differentiating (8) with respect to x and setting it to zero, one can see that the ν_g-parameter is strictly monotone for all linearly moving receivers on a path $g(x) = g_0 + g_1 x$, $x \geq d_O$, outside of a cone defined by

$$g_1 \in \begin{cases} \left(\frac{a_O - g_0}{d_O}, \frac{a_O - 2g_0}{d_O}\right) & \text{if } g_0 \leq 0 \\ \left(\frac{a_O - 2g_0}{d_O}, \frac{a_O - g_0}{d_O}\right) & \text{if } g_0 > 0 \end{cases}.$$

In particular, one boundary of the cone always passes the point (d_O, a_O). Indeed, $g_0 + \frac{a_O - g_0}{d_O} x|_{x = d_O} = a_O$. If $g_0 \leq 0$ or $g_0 > 0$, then ν_g has a local maxima or minima, respectively.

Now assume that g lies in the cone and $g_0 < 0$. We denote the coordinates of the global maxima with (p, q), $p > d_O$, where

$$p = \frac{-d_O g_0}{a_O - 2g_0 - d_O g_1},$$
$$q = 2\sigma(a_O - 2g_0 - d_O g_1)\sqrt{\frac{g_0(a_O - g_0 - d_O g_1)}{d_O}}.$$

After a normalization, $\hat{p} = \frac{p}{d_O}$ and $\hat{q} = \frac{q}{l}$, where $l = \lim_{x \to \infty} \nu_g(O, x) = \frac{a_O - d_O g_1}{\sqrt{dO}}$, these coordinates are independent of a scaling of the axes. Plugging $\hat{p}$ into $\hat{q}$ gives

$$\hat{q} = \frac{2\sqrt{\hat{p}^2 - \hat{p}}}{2\hat{p} - 1}. \tag{11}$$

The function $\hat{q}(\hat{p})$ is strictly increasing, positive and goes quite rapidly towards its limit 1, approximately like $\hat{q}(\hat{p}) \simeq 1 - (\hat{p} + 0.075)^{-4}$. In particular, the global maxima q of the function ν_g and the limit l differ by a large extent only in a very small region right behind the obstacle, e.g. for the example in the proof of Corollary II.14 (b) the region is $[3.2\ 3.20908]$. Furthermore, in this region the assumptions (4) used in the derivation of the ν parameter are not satisfied. Mathematically speaking this reduces to $\hat{q} \simeq 0 \Leftrightarrow l \simeq -\infty$ is equivalent to $\hat{p} \simeq 1 \Leftrightarrow p \simeq d_O$. On the other hand, if the receiver is in a region where the global maxima q is larger then the limit l, Equation (11) tells us that the ratio l/q will be approximately one. Mathematically speaking, $\hat{p} \gg 1 \Leftrightarrow p \gg d_O$ is equivalent to $\hat{q} \simeq 1 \Leftrightarrow q \simeq l$.

See Figure 4 for an instance of the cone, the corresponding behaviour of the function ν_g and the function $\hat{q}(\hat{p})$.

III. Deygout technique

Given some terrain profile $p(x)$, $x > 0$, $p(0) = 0$, a transmitter located at $T = (0, p(0))$ and a receiver located at $R = (d_R, a_R)$. We want to compute the diffraction loss at the receiver caused by the terrain $p(x)$.

Since this is a hard problem, one usually uses simplified solutions. In this paper we use the Deygout diffraction loss

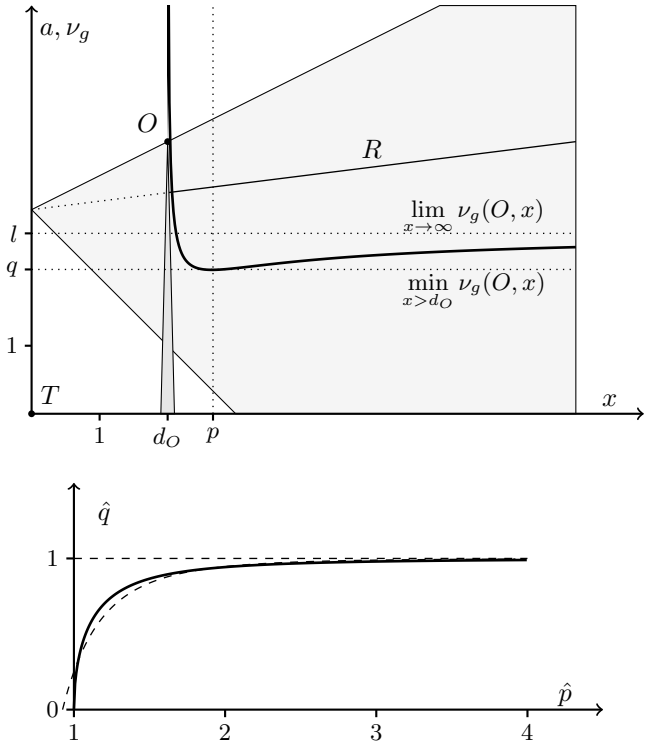

Fig. 4. (first) Illustration of the cone in Remark II.15. Given an obstacle $O = (2, 4)$ and a receiver R moving on the line $g(x) = 3 + x/8$. The shaded region includes all straight lines starting from $(0, 3)$, where the function ν_g is not strictly monotone, i.e. it has a local minima. The two dotted lines visualize the limit at infinity and the global minima of the function $\nu_g(O)$. The curved line is a plot of the function $\nu_g(O)$. Note, the cone in this example is not representative because $d_O \ll a_O$ and this case is excluded in our derivation of the formula of ν, see Section II.
(second) Plot of the function $\hat{q}(\hat{p})$, its limit 1 and an approximation $1 - (\hat{p} + 0.075)^{-4}$, the latter as a dashed line.

technique [7], although most of the developed techniques also apply directly to the Epstein–Peterson and the Giovanelli technique which also rely on the identification of main and secondary obstacles. The Deygout model assumes the presence of finitely many knife-edges between the transmitter and the receiver. As above, the obstacle with the highest ν-parameter is called the main-obstacle and its loss is calculated as for the single knife-edge model. Additional obstacles are identified between the transmitter and the top of the main obstacle, and the top of the main obstacle and the receiver, with losses calculated as for the single knife-edge model, see Figure 5. The total loss is the sum of all computed losses.

This technique can be iterated infinitely many times. But, no more than three obstacles should be considered with the Deygout-technique since the diffraction loss of a solid half plane, transmitter and receiver are sitting right on it, seems to be approximately 20 dB corresponding to [18, Figure 5], but the diffraction loss of four knife-edges with zero height is already greater than 20 dB. Indeed, by (5), $4 \cdot 20 \log_{10}(2) \simeq 24.08\,\text{dB} > 20\,\text{dB}$. Also, [19] suggests that only three obstacles should be used.

Before we proceed, we present a simple implementation computing the diffraction loss using the Deygout technique.

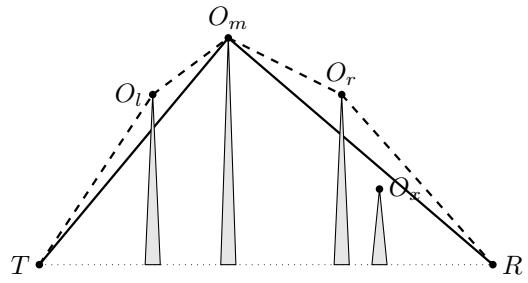

Fig. 5. Illustration of Deygout-method. T: Transmitter, R: Receiver, O_m: Main obstacle, O_l: Left secondary obstacle, O_r: Right secondary obstacle, O_x: ignored obstacle

Algorithm III.1 (Vanilla Deygout algorithm). [3]

Input Wavelength λ
Receiver $R = (d_R, a_R)$
Obstacles $O_j = (d_{O_j}, a_{O_j})$, $j = 1, \ldots, J$
Output diffraction loss L in dB

$j := 0,\ j_m := 0,\ \nu_m := -\infty$ //Search main obstacle
while $^{++}j < J$ and $d_{O_j} < d_R$ (12)
  $x = \nu(O_j, R)$
  if $x > \nu_m$ **then** $j_m := j,\ \nu_m := x$
$j := 0,\ j_l := 0,\ \nu_l := -\infty$ //Search left secondary obstacle
while $^{++}j < j_m$ (13)
  $x = \nu(O_j, O_{j_m})$
  if $x > \nu_l$ **then** $j_l := j,\ \nu_l := x$
$j := j_m,\ j_r := 0,\ \nu_r := -\infty$ //Search right sec. obstacle
while $^{++}j < J$ and $d_{O_j} < d_R$ (14)
  $x = \nu(O_j - O_{j_m}, R - O_{j_m})$
  if $x > \nu_r$ **then** $j_r := j,\ \nu_r := x$
$L = J(\sqrt{\frac{2}{\lambda}}\nu_m) + J(\sqrt{\frac{2}{\lambda}}\nu_l) + J(\sqrt{\frac{2}{\lambda}}\nu_r)$ //Sum losses (15)

A. Offline computation

Our first aim is to replace a given terrain profile with a finite set of knife-edges giving the same diffraction loss for the profile and a specific diffraction model by doing a ground profile analysis. So far, no rigorous mathematical profile analysis was performed but only heuristics [20]. We make the following light-headed definition.

Definition III.2. Given a diffraction model (in the following the Deygout model), and a *terrain profile*, or short *profile* $(x, p(x))$, $x > 0$, which is a piecewise linear function with edge points $P = \{p_n = (d_n, a_n) : n = 1, \ldots, N\}$, which may be regarded as a set of knife-edges at positions p_n, and a domain $V \subseteq \mathbb{R}^2$ whose points lie all above the profile.

A set (of knife-edges) $O = \{O_j : j = 1, \ldots, J\}$ is a *representer* for P and V if for all points (x, y) in the domain V the diffraction loss at (x, y) computed with respect to P and O is the same.

[3] The occurring function J is defined in (1).

Remark III.3. The identification of a given profile with knife-edges may not be optimal. It would certainly be worth to consider rounded obstacles whose curvature is determined by the given profile, see e.g. [21], [22].

The idea of the inverse Deygout algorithm is, to add all profile points to the representer which are main and secondary obstacles for any point (x, y) in the domain V above the profile.

Theorem III.4. *Given a profile $P = \{(d_n, a_n) : n = 1, \dots, N_P\}$, and a convex, bounded, polytope $V \subseteq \mathbb{R}^2$ with vertices v_n, $n = 1, \dots, N_V$. Let $\nu_p(v) = \nu(p, v)$ be the ν-parameter of obstacle $p \in P$ and vertex $v \in V$.*

Define the sets O_m, O_l, O_r by

$$\begin{aligned} p_m \in O_m \quad & \text{if} \quad \max_{v\in V} \nu_{p_m}(v) \geq \min_{v\in V} \nu_p(v) \\ & \text{for all } p \in P \\ p_l \in O_l \quad & \text{if} \quad \nu_{p_l}(o_m) \geq \nu_p(o_m), \\ & o_m \in O_m \text{ and for all } p \in P \\ p_r \in O_r \quad & \text{if} \quad \max_{v\in V} \nu_{p_r - o_m}(v - o_m) \geq \min_{v\in V} \nu_{p-o_m}(v - o_m), \\ & o_m \in O_m \text{ and for all } p \in P, \end{aligned}$$

where we defined $v - o = (d_v - d_o, a_v - a_o)$.

Then the set $O_m \cup O_l \cup O_r$ is a, not necessarily minimal, representer for P and V for the Deygout diffraction model and for all NLoS points.

The set O_m contains all main obstacles of points in the polytope V, the set O_l contains all secondary obstacles left of a main obstacle o_m, The set O_r contains all secondary obstacles right of a main obstacle o_m which is why need to shift the position of the transmitter and the obstacle by o_m.

Proof. This follows directly from Corollary II.10. □

An algorithm based on Theorem III.4 has complexity roughly $O(4N_P N_V)$, since for each section of the profile P one has to compute 4 ν-parameters per vertex v_n, $n = 1, \dots, N$. Since some computations are redundant one can reduce the complexity easily to $O(\frac{5}{2} N_P N_V)$. However, this computation can be done offline, and thus, its complexity does not matter much.

A bigger problem is that an algorithm based on Theorem III.4 yields too many false positives, implying that the representer is not minimal. Using Theorem II.14 (b), or better Remark **??**, we can reduce the number of false positives to a large extent.

Theorem III.5. *Assume that Corollary II.14 (b) is true for our profile P and polytope V, where P and V is defined as in III.4. If for some $p_m \in P$*

$$\nu_{p_m}(v) \geq \nu_p(v) \text{ for all } p \in P,\ v \in V \tag{16}$$

then $O_m = \{p_m\}$ is the set of all main obstacles for all points in V. Otherwise, define O_m as in Theorem III.4. If for some $p_r \in P$

$$\nu_{p_r - o_m}(v - o_m) \geq \nu_{p-o_m}(v - o_m) \text{ for all } p \in P,\ v \in V$$

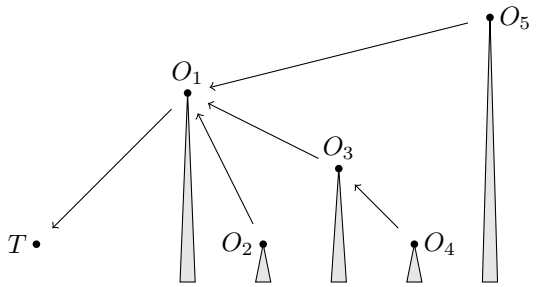

Fig. 6. Illustration of the indices corresponding to the convex hull as defined in Algorithm III.9. Given Obstacles $O_1 = (2, 2)$, $O_2 = (3, 0)$, $O_3 = (4, 1)$, $O_4 = (5, 0)$ and $O_5 = (6, 3)$, we get the the indices $i_1 = 0$, $i_2 = 1$, $i_3 = 1$, $i_4 = 3$ and $i_5 = 1$.

then $\{p_r\}$ is the set of all right secondary obstacles for the set O_m. Otherwise, define O_r as in Theorem III.4. Furthermore, define O_l as in Theorem III.4.

Then, the set $O_m \cup O_l \cup O_r$ is a representer for P and V.

Remark III.6. Whenever Theorem III.4 returns a set of obstacles which contradicts Corollary II.12, whenever for some polytope (16) is not fulfilled, we can subdivide the polytope into finitely smaller polytopes and compute a representer for each smaller polytope.

B. Online computation

Given a representer O, we now discuss how to speed up the computation of the diffraction loss. We first discuss replacements for the function ν to reduce the computational load inside the loops (12), (13), (14).

Remark III.7. To reduce the costs of the computation of the ν-parameters,

$$\nu = \frac{a_O d_R - d_O a_R}{\sqrt{d_R d_O (d_R - d_O)}},$$

one may use the function ν_2, defined by

$$\begin{aligned} \nu_2 &= \frac{x \cdot |x|}{d_R d_O (d_R - d_O)}, \text{ where} \\ x &= a_O d_R - d_O a_R, \end{aligned}$$

to avoid the cost of taking the square root. To compute ν_2 one has to do 5 multiplications and 2 summations. Clearly, all statements in this paper holding for ν also hold for ν_2.

It may also be useful to use the function ν_5, taking 5 parameters, defined by

$$\begin{aligned} \nu_5 &= \frac{x \cdot |x|}{e_R d_O (d_R - d_O)}, \text{ where} \\ x &= a_O - d_O k_R, \quad e_R = \frac{1}{d_R}, \quad k_R = a_R e_R. \end{aligned}$$

To compute ν_5 one has to do only 4 multiplications and 2 summations, since the computation of k_R and e_R can be done outside the loop.

If the function ν is replaced by one of the above, one has to replace the computation of the diffraction loss in (15) accordingly, namely

$$L = J(\hat{\nu}_m) + J(\hat{\nu}_l) + J(\hat{\nu}_r), \text{where}$$

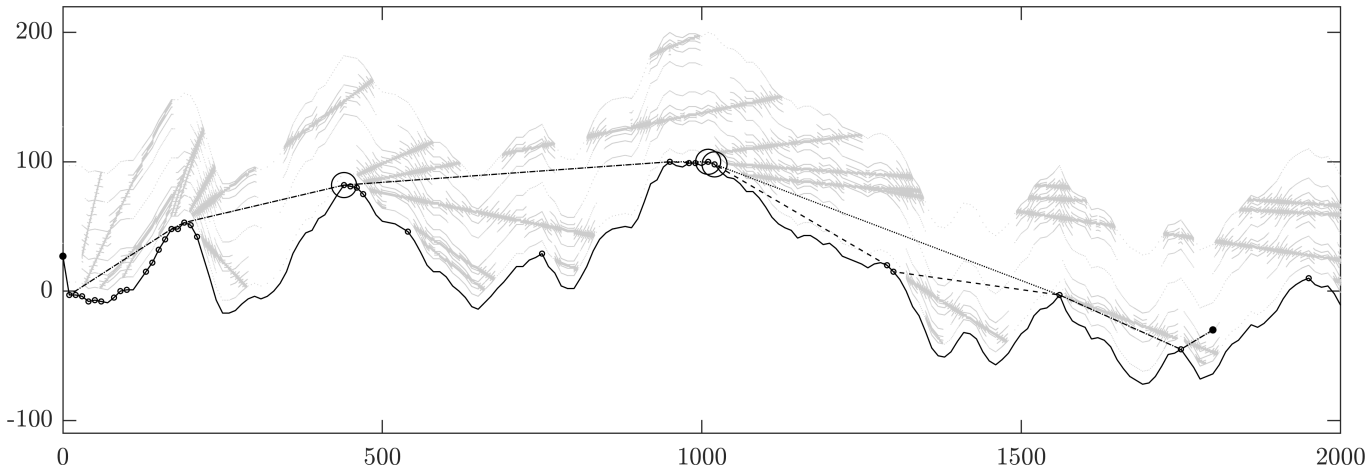

Fig. 7. Plotted is a random terrain in black, the vertices of the quadrilaterals defining the the positions of the receivers in light grey and the identified representer as small circles. Furthermore, a receiver and transmitter as a large dot, the identified main, left and right obstacle as large circles and lines connecting the considered obstacles in the computation of the main left and right obstacles (corresponding to the set of indices i_j) of the receivers as dotted, dashed and dashed lines respectively.
Note though, the representer contains a lot of obstacles near to the transmitter, since all of these points are LoS with no obstacle in front of them. In a productive implementation one may only consider obstacles with minimal ν parameter of -0.78.

$$\hat{\nu}_\circ = \sqrt{\tfrac{2}{\lambda}} \cdot \sigma(\nu_\circ)\sqrt{|\nu_\circ|}, \quad \circ \in \{m, l, r\}.$$

We now make use of Corollary II.12. which reduces the number of ν parameters one has to compute.

Definition III.8. Given a transmitter T, obstacles $O = \{O_j : j = 1, \dots, J\}$ and let I be indices of the obstacles which belong the upper boundary of the convex hull of $T \cup O$. For O_J we define i_J as the largest j, $j < J$, such that $j \in I_J$. If there is no such value, we set it to zero.

Note that the indices i_j from Definition III.8 can be precomputed, since they only depend on the obstacles. See Figure 6 for a visual explanation.

Algorithm III.9 (Revised Deygout algorithm)**.** We only show how to compute the main obstacle and its corresponding ν parameter and do not give the full algorithm.

Input Wavelength λ
Receiver $R = (d_R, a_R)$
Obstacles $O_j = (d_{O_j}, a_{O_j})$, $j = 1, \dots, J$
Indices i_j, $j = 1, \dots, J$
Output diffraction loss L in dB

Search $\tilde{J} \leq J$ such that $d_{O_{\tilde{J}}} < d_R < d_{O_{\tilde{J}+1}}$. (17)
$j := \tilde{J},\ j_m := 0,\ \nu_m := -\infty$ //Search main obstacle
while $j \neq 0$
  $x = \nu(O_j, R)$
  if $x > \nu_m$ **then** $j_m := j,\ \nu_m := x$
  if $\nu_m > 0$ **then** $j := i_j$ **else** $j := j - 1$ (18)
...

We shortly discuss the two main differences in the revised algorithm, marked with (17) and (18).

(17) Instead with starting to search for the main obstacle from the beginning, we start from the end. Thus, we first have to search for the last obstacle $O_{\tilde{J}}$ which is still in front of the receiver. Under our standing assumption that the obstacles O_j are sorted with respect to d_{O_j}, this takes $O(\log J)$ operations.

(18) If our receiver is NLoS, then we can follow the indices i_j back to the transmitter on our search for the main obstacle. If our receiver is LoS, and since we are not given indices corresponding to the "LoS-convex hull", we cannot follow any faster path back to the transmitter and just advance by one.

In Figure 8 one can see the efficiency of the revised Deygout algorithm compared to the vanilla Deygout algorithm. One can clearly see that the more points the profile has and the hillier it is, the larger are the savings using the revised Deygout algorithm.

IV. Conclusion

We illustrated and proved that the revised Deygout algorithm is equivalent to the original Deygout algorithm, but has much less computational complexity and memory consumption.[4] The methods are fully flexible and comprehensively applicable to terrestrial and non-terrestrial wireless systems such as 5G and beyond. Furthermore, the revised Deygout algorithm can be efficiently integrated in real-time applications to perform diffraction loss estimations. We demonstrated the applicability for BVLoS UAV operations as a use-case scenario and also integrated the proposed methods into our highly scalable software system. As a next step we investigate whether a similar approach can be taken for scattering and reflection effects.

Acknowledgements

The authors are grateful to Thomas Wana for feedback on the algorithm and to Thomas Neubauer for insightful remarks and suggestions.

[4]In case of further interest a code implementation can be provided upon request - please reach out to office@dimetor.com or the authors.

Profile	N	vanilla	offline	revised
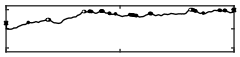	402	801	97	34
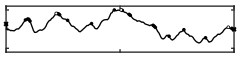	202	401	55	8
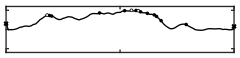	102	201	27	20
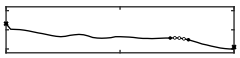	39	75	9	7
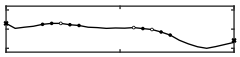	27	53	19	14
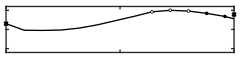	14	23	9	9

Fig. 8. Number of operations needed to compute the diffraction loss using various algorithms. We report the • approximate shape of the profile (the ticks are located at $0m$, $1000m$, $2000m$ and $-100m$, $0m$, $100m$ in the in the x-direction and y-direction, respectively; the main, left and right obstacles are marked as white dots, the identified representer is marked with black dots, the transmitter and receiver are marked by $\times$ and are located at the leftmost and rightmost point of the profile, respectively), • number of points of the profile N, • diffraction loss J and the number of ν-parameters needed to compute using the algorithms • vanilla Deygout, • vanilla Deygout using offline computational steps and • revised Deygout using offline computational steps.

REFERENCES

[1] GSMA, *Using Mobile Networks to Coordinate Unmanned Aircraft Traffic*, Tech. Rep., (2018).

[2] EUROCONTROL, *Roadmap for the integration of civil Remotely-Piloted Aircraft Systems into the European Aviation Systems*, (2013).

[3] FAA, *Integration of Civil Unmanned Aircraft Systems (UAS) in the National Airspace System (UAS) Roadmap*, Tech. Rep., (2013).

[4] *UTM*, (2020), faa.gov/uas/research_development/traffic_management.

[5] Dimetor, *AirborneRF*, (2020), dimetor.com.

[6] L. Anderson, L. Trolese, *Simplified method for computing knife edge diffraction in the shadow region*, IEEE Trans. Antenn. Propag., (1958).

[7] J. Deygout, *Multiple knife-edge diffraction of microwaves*, IEEE Trans. Antennas Propag., 14 (1966) 4.

[8] J. Epstein, D. W. Peterson, *An experimental study of wave propagation at 850 MC*, Proc. IRE, 41 (1953) 5.

[9] C. L. Giovanelli, *An analysis of simplified solutions for multiple knife-edge diffraction*, IEEE Trans. Antennas Propag., 32 (1984) 3.

[10] I. Popescu, M. Nafornita, A. Voulgarelis, P. Constantinou, *Applications of neural networks to the prediction of propagation path loss for mobile communications systems*, Proc. of the Second International Symposium of Trans Black Sea Region on Applied Electromagnetism, (2000).

[11] C. Tzaras, S. R. Saunders, *Comparison of multiple-diffraction models for digital broadcasting coverage prediction*, IEEE Trans. Broadcast., 46 (2000) 3.

[12] V. Nguyen, H. Phan, A. Mansour, A. Coatanhay, *VoglerNet: multiple knife-edge diffraction using deep neural network*, 14^{th} European Conference on Antennas and Propagation, Copenhagen, Denmark, (2020).

[13] C. Lee, S. Park, *An approach of the diffraction loss prediction using artificial neural network in hilly mountainous terrain*, Microw. Opt. Technol. Lett., 59 (2017).

[14] R. Mathar, T. Rick, *Fast Edge-Diffraction-Based Radio Wave Propagation Model for Graphics Hardware*, 2^{nd} International ITG Conference on Antennas, Munich, (2007).

[18] J. H. Whitteker, *Diffraction over a flat-topped terrain obstacle* IEEE Proceed., 137 (1990) 2.

[15] T. S. Rappaport, *Wireless Communications - Principles and Practice*, Prentice-Hall, Inc., 2002.

[16] W. C. Y. Lee, *Mobile Cellular Telecommunications Systems*, McGraw Hill Publications, New York, 1989.

[17] ITU, *Recommendation ITU-R P.526-15, Propagation by diffraction*, (2019).

[19] N. DeMinco, P. McKenna, *A comparative analysis of multiple knife-edge diffraction methods*, Proc. ISART/ClimDiff, (2008).

[20] P. Angueira, A. Arrinda, J. L. Ordiales, D. De la Vega, M. M. Vélez, P., A. S. Vicente, *Ground profile analysis algorithm to improve multiple diffraction loss estimation*, In: Proceedings Of The International Symposium On Antennas And Propagation, Japan, 3 (2000)..

[21] M. S. De Assis, *A simplified solution to the problem of multiple diffraction over rounded obstacles*, IEEE Trans. Antennas Propag., 19 (1971) 2.

[22] H. T. Dougherty,, L. J. Maloney, *Application of diffractions by convex surfaces to irregular terrain situations*, J. Res. Nat. Bur. Stand., (1964).

Thomas Mejstrik received his Master in piano studies from University of music and performing arts Vienna and earned his Ph.D. in Mathematics for work on joint spectral radius and subdivision schemes from the University of Vienna, Austria, in 2019. Since 2019 he is researcher at Dimetor GmbH and since 2020 post doc at the University of Vienna, Austria. His interests lie in multiple subdivision schemes, wireless networks and music.

Taulant Berisha holds a BS (2011), a MS (2014) in Electrical Engineering from the University of Prishtina, Kosovo, and Ph.D. (2019) in Telecommunications from TU Wien, Austria. From 2015–2019 he was a project assistant at TU Wien, and since 2019 he is a researcher at Dimetor GmbH. His research interests are vehicular communications, BVLoS UAV operations, benchmarking, statistical modelling and service quality measurements.

Sebastian Woblistin received his Ph.D in Mathematics from the University of Vienna in 2017, working on analytic varieties in power series spaces, Artin approximation and infinite-dimensional complex analysis. Since 2016 he has been working as a software developer and since 2018 he is a researcher and senior software developer at Dimetor GmbH, working on high-performance radio propagation modelling in the context of UAV operations.